

Angewandte Chemie

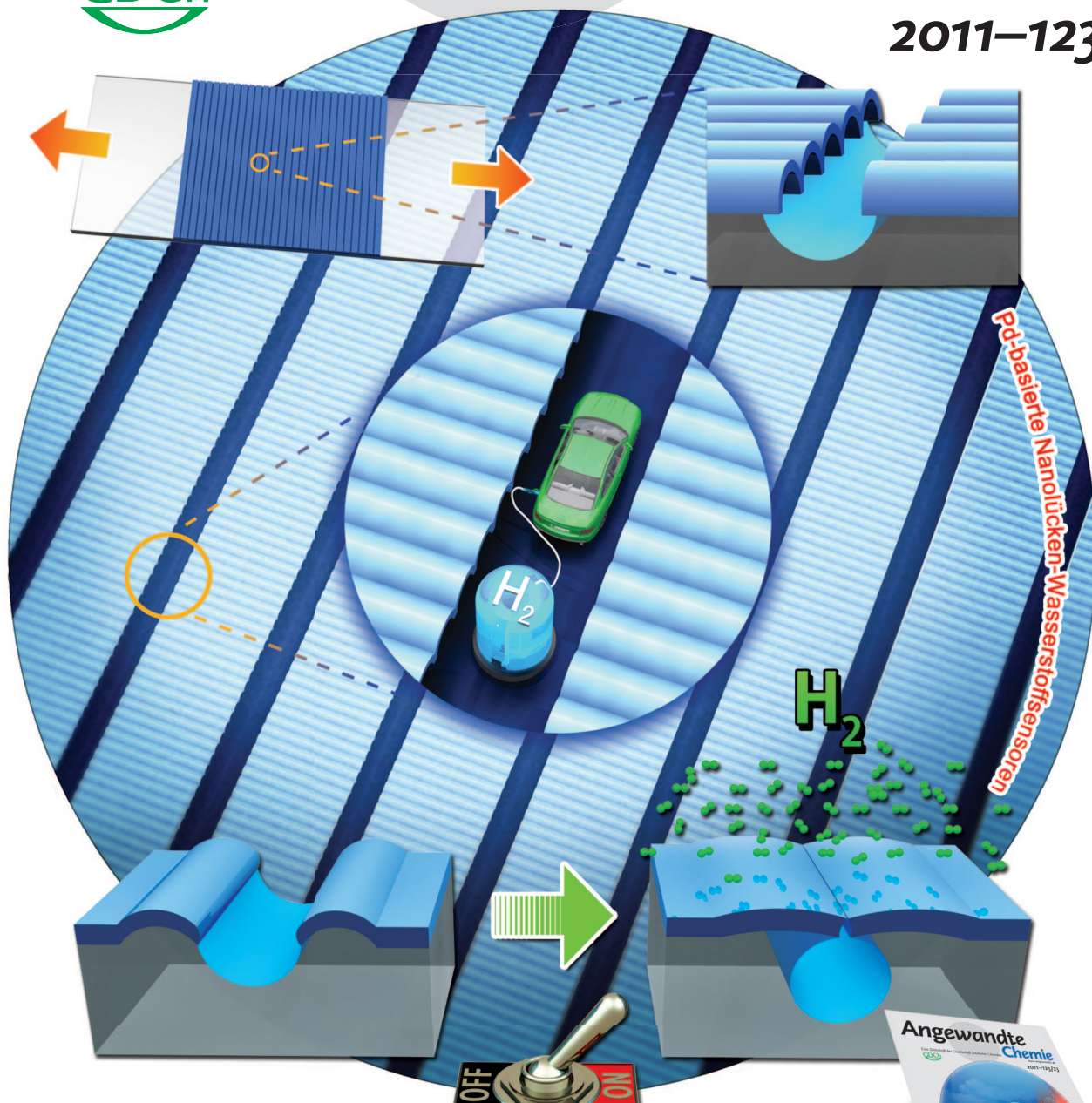
D 1331

Eine Zeitschrift der Gesellschaft Deutscher Chemiker

GDCh

www.angewandte.de

2011–123/23



Mikroskopie mit Doughnut-Moden

A. J. Meixner et al.

Hydratisiertes Elektron

B. Abel und K. R. Siefemann

**Highlights: Massenspektrometrie • Ferndetektions-NMR •
Einzelmolekülspektroskopie**

ANCEAD 123 (23) 5335–5514 (2011) · ISSN 0044–8249 · Vol. 123 · No. 23

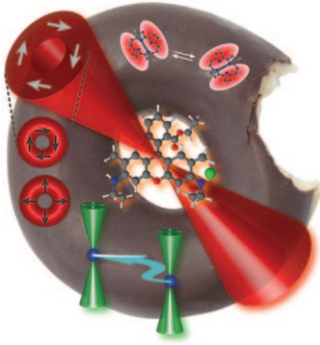
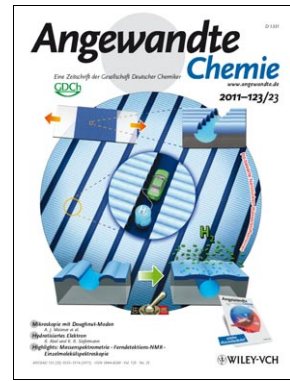


 WILEY-VCH

Titelbild

Junmin Lee, Wooyoung Shim, Eunyeong Lee, Jin-Seo Noh und Wooyoung Lee*

Eine lithographiefreie nanolückenbasierte Chemosensormethode nutzt die Bildung von Brüchen in einem dünnen Pd- oder PdNi-Film, die durch Strecken des Films auf einem Elastomersubstrat erzeugt wurden. Diese preiswerte, skalierbare Methode, die auf einem hoch mobilen dünnen Film auf einem Elastomer (MOTIFE) beruht, liefert zuverlässige und hoch empfindliche H₂-Sensoren, wie W. Lee et al. in der Zuschrift auf S. 5413 ff. zeigen.

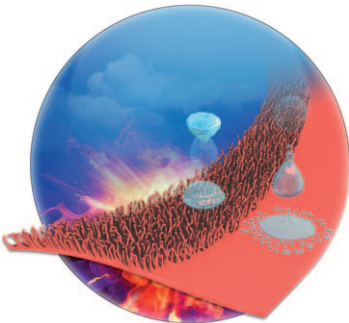
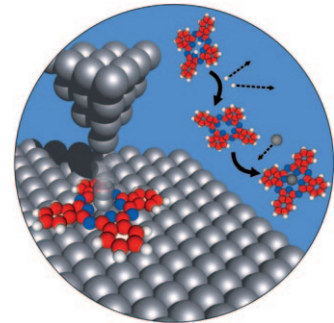


Mikroskopie mit Doughnut-Moden

Lasermode mit ringförmigem Strahlprofil – Doughnut-Moden – finden Anwendung in den Bio- und Materialwissenschaften oder der Einzelmolekülmikroskopie, ihr gesamtes Potential ist aber noch längst nicht ausgeschöpft. Im Aufsatz auf S. 5384 ff. fassen A. J. Meixner et al. den Stand der Forschung zusammen und blicken in die Zukunft dieser Technik.

Phthalocyanine

R. Berndt et al. beschreiben in der Zuschrift auf S. 5406 ff. die kontrollierte Metallierung einzelner Phthalocyaninmoleküle auf einer Silberoberfläche mithilfe eines Rastertunnelmikroskops.



Benetzungsarten

Der Wechsel von Wassertropfen vom Spreiten zum Abprellen auf hydrophilen, hydrophoben, superhydrophilen und superhydrophoben heißen Oberflächen wird von J. Wang, L. Jiang et al. in der Zuschrift auf S. 5423 ff. untersucht.



The following Communications have been judged by at least two referees to be “very important papers” and will be published online at www.angewandte.org soon:

I. Garcia-Bosch, A. Company, C. W. Cady, S. Styring, W. R. Browne, X. Ribas, M. Costas*

Evidence for a Precursor Complex in C–H Hydrogen-Atom-Transfer Reactions Mediated by a Manganese(IV) Oxo Complex

G. N. Newton, S. Yamashita, K. Hasumi, J. Matsuno, N. Yoshida, M. Nihei, T. Shiga, M. Nakano, H. Nojiri, W. Wernsdorfer, H. Oshio*

Redox-Controlled Optimization of the Magnetic Properties of Keggin-Type {Mn₁₃} Clusters

C. C. Lee, Y. Hu,* M. W. Ribbe*

Tracing the Hydrogen Source of Hydrocarbons Formed by Vanadium Nitrogenase

S. R. Waldvogel,* J. Kulisch, M. Nieger, F. Stecker, A. Fischer
Efficient and Stereodiverse Electrochemical Synthesis of Optically Pure Menthylamines

J. Liu, S. Z. Qiao,* H. Liu, J. Chen, A. Orpe, D. Zhao, G. Q. Lu*
Extension of the Stöber Method to the Preparation of Monodisperse Spheres of Resorcinol–Formaldehyde Resin Polymer and Carbon

T. Lewis, M. Faubel, B. Winter, J. C. Hemminger*

CO₂ Capture in an Aqueous Solution of an Amine: Role of the Solution Interface

Y. H. Kim, S. Banta*

Complete Oxidation of Methanol in an Enzymatic Biofuel Cell by a Self-Assembling Hydrogel Created from Three Modified Dehydrogenases

R. B. Bedford,* M. F. Haddow, C. J. Mitchell, R. L. Webster
Mild C–H Halogenation of Anilides and the Isolation of an Unusual Pd^I–Pd^{II} Species

W. Gan, B. Xu, H.-L. Dai*

Activation of Reactions of Thiols at the Silver-Nanoparticle Surface

M. Sasaki, Y. Kondo, M. Kawahata, K. Yamaguchi, K. Takeda*
Enantioselective Synthesis of Siloxyallenes from Alkynoyl Silanes by Reduction and a Brook Rearrangement and Their Subsequent Trapping in a [4+2] Cycloaddition with Unusual Facial Selectivity

H. S. Choi, K. Nasr, S. Alyabyev, D. Feith, J. H. Lee, S. H. Kim, Y. Ashitate, H. Hyun, G. Patonay, L. Strekowski, M. Henary,* J. V. Frangioni*

Zwitterionic Near-Infrared Fluorophores and Their Fate In Vivo

Author Profile



“When I was eighteen I wanted to be a professional tennis player.

When I wake up I wake up my 8-year-old son ...”

This and more about Guy Bertrand can be found on page 5248.

Guy Bertrand _____ 5248 – 5250

Obituaries

Gernot Boche (1938–2011)

R. W. Hoffmann,
M. Famulok* _____ 5251 – 5252

Books

From Non-Covalent Assemblies to Molecular Machines

Jean-Pierre Sauvage, Pierre Gaspard

reviewed by J. Nitschke _____ 5254

High Energy Density Lithium Batteries

Katerina E. Aifantis, Stephen A. Hackney,
R. Vasant Kumar

reviewed by B. Scrosati _____ 5254

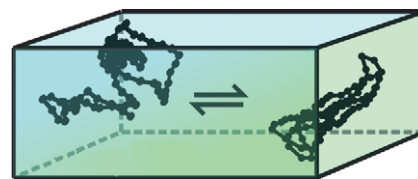
Highlights

Polymer Processing

F. A. Feist, T. Basché* — 5256 – 5257

The Folding of Individual Conjugated Polymer Chains during Annealing

Chain reaction: Single-molecule spectroscopy can be used for the real-time observation of the translational and conformational dynamics of individual conjugated polymer chains during the annealing of solid films. Thus, a detailed molecular understanding of annealing mechanisms is at hand.

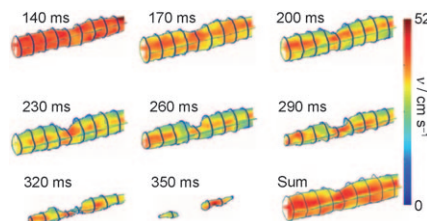


Remote Detection

E. Paciok, B. Blümich* — 5258 – 5260

Ultrafast Microscopy of Microfluidics: Compressed Sensing and Remote Detection

Zooming in on microfluidics: The potential of conventional NMR microscopy is limited by poor sensitivity and long measurement times. Recent advances in remote-detection NMR spectroscopy overcome these limitations and give unique insight into microfluidic processes with unprecedented spatial and temporal resolution (picture: high-resolution three-dimensional velocity maps of fast flow in a microcapillary).



Mass Spectrometry

F. Coelho,* M. N. Eberlin* — 5261 – 5263

The Bridge Connecting Gas-Phase and Solution Chemistries



Charged wings for flying fish: Mass spectrometry allows the investigation of chemical reactions at the molecular level with ease, speed, selectivity, sensitivity, and great flexibility. Modern mass spectrometry provides a bridge that allows chemical reactions that occur in the gas phase to be studied in solution, and vice-versa (see picture).

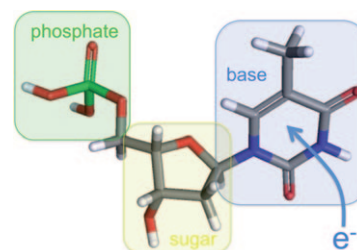
Minireviews

Electrons in Water

K. R. Siefertmann, B. Abel* — 5264 – 5272

The Hydrated Electron: A Seemingly Familiar Chemical and Biological Transient

Two recent milestones in the research of the hydrated electron were the determination of its vertical binding energy and the discovery of a long-lived hydrated electron near the surface of liquid water. The results bear relevance for many fields, e.g., electron attachment to DNA bases (see picture).



For the USA and Canada: ANGEWANDTE CHEMIE International Edition (ISSN 1433-7851) is published weekly by Wiley-VCH, PO Box 191161, 69451 Weinheim, Germany. Air freight and mailing in the USA by Publications Expediting Inc., 200 Meacham Ave., Elmont, NY 11003. Periodicals

postage paid at Jamaica, NY 11431. US POSTMASTER: send address changes to *Angewandte Chemie*, Journal Customer Services, John Wiley & Sons Inc., 350 Main St., Malden, MA 02148-5020. Annual subscription price for institutions: US\$ 9442/8583 (valid for print and electronic / print or electronic delivery); for

individuals who are personal members of a national chemical society prices are available on request. Postage and handling charges included. All prices are subject to local VAT/sales tax.

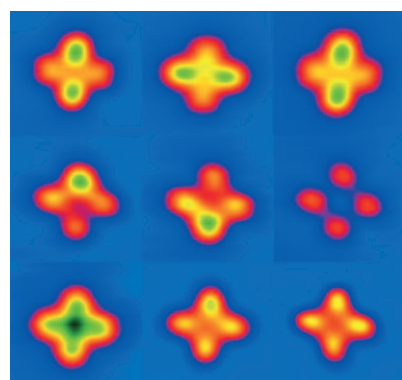
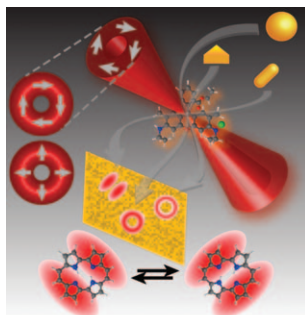
Reviews

Microscopy Techniques

T. Züchner, A. V. Failla,
A. J. Meixner* _____ 5274–5293

Light Microscopy with Doughnut Modes:
A Concept to Detect, Characterize, and
Manipulate Individual Nanoobjects

Doughnuts for nanotechnology: Higher-order laser modes with a doughnut-shape and a tunable polarization (see picture) have an extraordinary potential for new applications in nanotechnology. They already serve as versatile tools in microscopy and are finding use in many fields of science from pure optics to different branches of applied science including bio- and materials science.



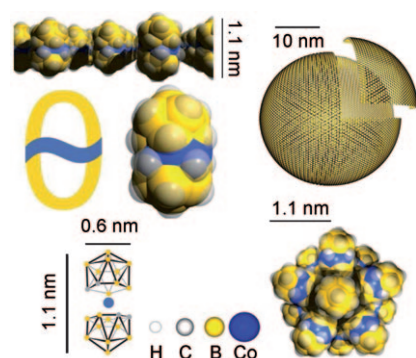
Silvered molecules: The controlled metalation of individual phthalocyanine (H_2Pc) molecules to form $AgPc$ was observed by low-temperature scanning tunneling microscopy (STM). Stepwise dehydrogenation was followed by Ag^+ implantation; tautomerization and hydrogen atom hopping within the H_2Pc inner ring were also induced by electron injection from the STM tip.

Communications

Surface Chemistry

A. Sperl, J. Kröger,
R. Berndt* _____ 5294–5297

Controlled Metalation of a Single
Adsorbed Phthalocyanine



Sandwiched: The cobaltabisdicarbollide (mono-)anion ($[3,3'-Co(1,2-C_2B_9H_{11})_2]^-$, $COSAN^-$) forms monolayer vesicles at low concentrations in water (see picture). An increase in concentration leads to a Coulomb explosion of the closely packed vesicles into small micelles, which results in the coexistence of both aggregation states at higher concentrations.

Vesicles

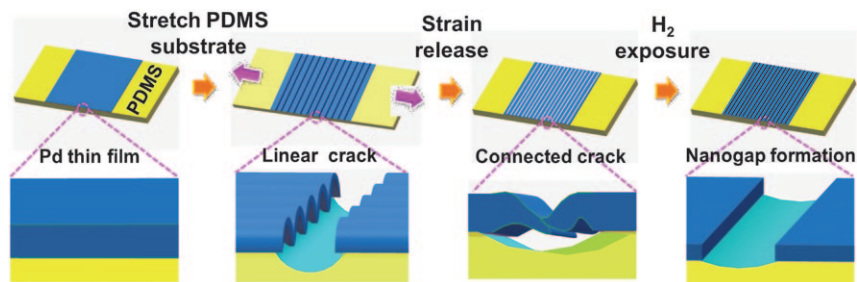
P. Bauduin,* S. Prevost, P. Farràs,
F. Teixidor, O. Diat, T. Zemb _____ 5298–5300

A Theta-Shaped Amphiphilic
Cobaltabisdicarbollide Anion: Transition
From Monolayer Vesicles to Micelles

VIP Chemical Sensors

J. Lee, W. Shim, E. Lee, J.-S. Noh,
W. Lee* _____ 5301–5305

Highly Mobile Palladium Thin Films on an Elastomeric Substrate: Nanogap-Based Hydrogen Gas Sensors



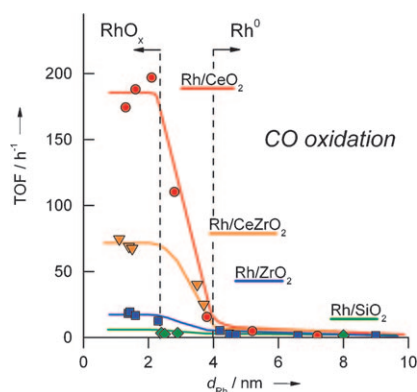
MOTIFE chemical sensors: A novel, low-cost, scalable, and lithography-free but nanogap-based chemical sensing method is presented. This method, termed highly-mobile thin film on elastomer (MOTIFE),

utilizes crack formation in a Pd and PdNi thin film generated by stretching the film on an elastomeric substrate to reliably and reproducibly provide highly sensitive H₂ sensors.

CO Oxidation

D. A. J. M. Ligthart, R. A. van Santen,
E. J. M. Hensen* _____ 5306–5310

Supported Rhodium Oxide Nanoparticles as Highly Active CO Oxidation Catalysts

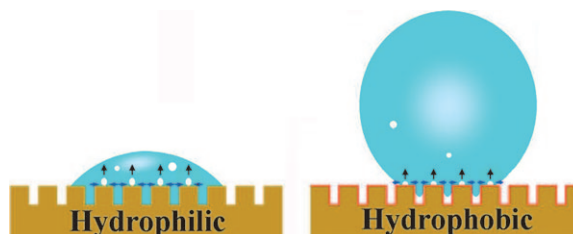


Bigger is not always better: Rhodium metal particles smaller than 2.5 nm are oxidized and stabilized by reducible supports such as ceria under CO oxidation conditions, whereas metal particles larger than 4 nm remain metallic. The very small Rh oxide particles are more active by two orders of magnitude in CO oxidation than Rh metal particles (see picture; TOF = turnover frequency).

VIP Surface Chemistry

T. Zhang, J. Wang,* L. Chen, J. Zhai,
Y. Song, L. Jiang* _____ 5311–5314

High-Temperature Wetting Transition on Micro- and Nanostructured Surfaces



Wet, wet, wet: Typical wetting transition (from spreading to bouncing) of water droplets on micro- and nanostructured surfaces at high temperatures has been investigated. The spreading and bouncing behavior varies on substrates with differ-

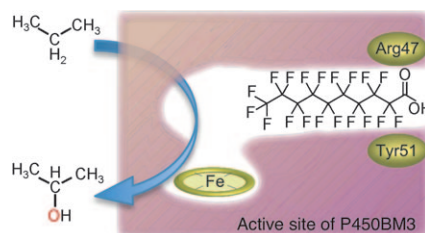
ent wettabilities (see picture; substrate brown, water droplet blue, water vapor white), and the bouncing temperature changes when the microstructure of the surface changes.

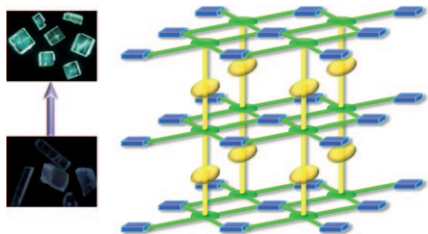
Alkane Activation

N. Kawakami, O. Shoji,
Y. Watanabe* _____ 5315–5318

Use of Perfluorocarboxylic Acids To Trick Cytochrome P450BM3 into Initiating the Hydroxylation of Gaseous Alkanes

It has long been believed that the fatty acid hydroxylase wild-type P450BM3 is unable to oxidize gaseous alkanes. However, the simple addition of a perfluorocarboxylic acid as a dummy substrate to initiate the P450BM3 catalytic cycle enabled the efficient hydroxylation of butane and propane (see picture).





The same but different: Four samples of an organic zinc phosphate hybrid material prepared at four different temperatures have the same structure but show distinct luminescence (see pictures of two of the samples).

Luminescent Materials

S. H. Huang, S. L. Wang* — 5319–5322

Variant Luminescence from an Organic–Inorganic Hybrid Structure with an Isolated 4-Ring Zinc Phosphate Tecton



Mothball macrocycles: Naphthalene has been coupled to form macrocyclic oligomers composed of five, six, and seven naphthalene units (see picture). Thermally stable macrocycles bearing 50, 60,

or 70 π electrons within the hydrocarbon structure form columnar assemblies in crystals and serve as bipolar carrier transport materials in organic light-emitting diode devices.

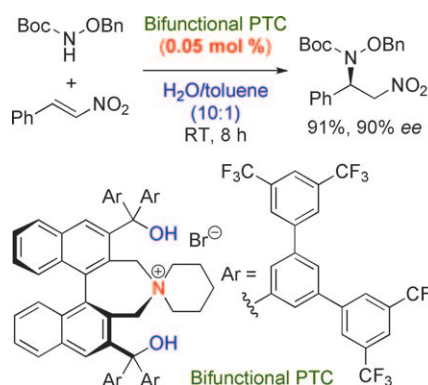
Organic Materials

W. Nakanishi, T. Yoshioka, H. Taka, J. Y. Xue, H. Kita, H. Isobe* . 5323–5326

[*n*]Cyclo-2,7-naphthylenes: Synthesis and Isolation of Macrocyclic Aromatic Hydrocarbons having Bipolar Carrier Transport Ability



It's just a phase: Environmentally benign title reaction was achieved under neutral phase-transfer conditions in the presence of 0.05 mol % of a chiral bifunctional ammonium bromide. The importance of bifunctional design of the chiral phase-transfer catalysts (PTC) was clearly shown in the transition-state model of the reaction based on the single-crystal X-ray structure. Bn = benzyl, Boc = *tert*-butoxycarbonyl.



Phase-Transfer Catalysis

L. Wang, S. Shirakawa, K. Maruoka* — 5327–5330

Asymmetric Neutral Amination of Nitroolefins Catalyzed by Chiral Bifunctional Ammonium Salts in Water-Rich Biphasic Solvent



It's the iodine: The intra- and intermolecular title reaction is catalyzed by an in situ generated ammonium (hypo)iodite species. Either H_2O_2 or *tert*-butyl hydroperoxide (TBHP) can be used as an environ-

mentally benign oxidant and a wide range of substrates react to give the corresponding α -acyloxycarbonyl compounds in good to excellent yields.

Oxidation


M. Uyanik, D. Suzuki, T. Yasui, K. Ishihara* — 5331–5334

In Situ Generated (Hypo)iodite Catalysts for the Direct α -Oxyacylation of Carbonyl Compounds with Carboxylic Acids

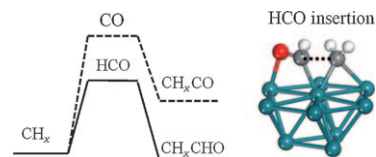


Syngas Chemistry

Y. H. Zhao, K. J. Sun, X. F. Ma, J. X. Liu, D. P. Sun, H. Y. Su, W. X. Li* **5335–5338**


 Carbon Chain Growth by Formyl Insertion on Rhodium and Cobalt Catalysts in Syngas Conversion

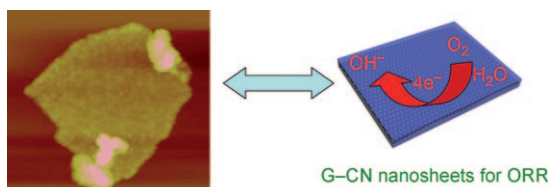
HCO insertion into CH_x exhibits superior or similar activity to CO insertion and carbene coupling according to DFT calculations, which thus reveal a new reaction channel for chain growth in syngas conversion. The picture shows schematically the lower reaction barrier for HCO versus CO insertion and the optimized transition state for insertion of HCO into CH_2 .



Metal-Free Electrocatalysts

S. Yang, X. Feng,* X. Wang, K. Müllen* **5339–5343**

 Graphene-Based Carbon Nitride Nanosheets as Efficient Metal-Free Electrocatalysts for Oxygen Reduction Reactions




Sandwich-like, graphene-based carbon nitride nanosheets (G-CN), among many other advantages, show an enhanced electrical conductivity. Oxygen atoms can thus access the catalyst surface easily and the rapid diffusion of electrons in the

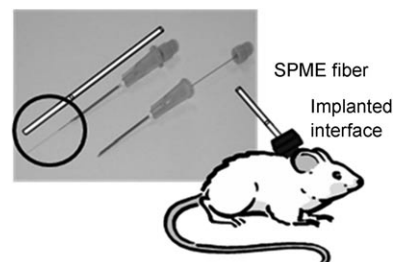
electrode during the oxygen reduction process is facilitated. G-CN nanosheets can hence serve as metal-free electrocatalysts for oxygen reduction reactions (ORR) with excellent performance.

Analytical Methods

D. Vuckovic, I. de Lannoy, B. Gien, R. E. Shirey, L. M. Sidisky, S. Dutta, J. Pawliszyn* **5344–5348**

 In Vivo Solid-Phase Microextraction: Capturing the Elusive Portion of Metabolome

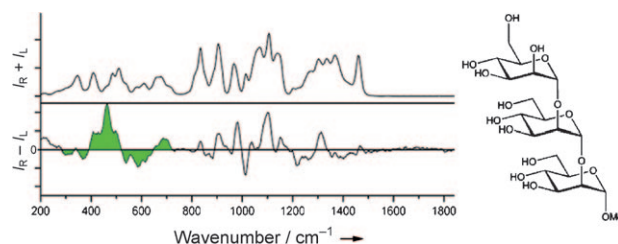
Metabolites with fast turnover rates and/or unstable metabolites can be captured directly from circulating blood using a new solid-phase microextraction (SPME) device based on a hypodermic needle. Such metabolites are not observed using solvent precipitation and ultrafiltration methods, indicating traditional approaches based on blood withdrawal are not adequately capturing complete metabolome at the time of sampling.



Glycoproteins

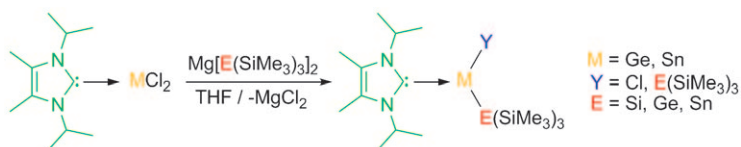
C. Johannessen, R. Pendrill, G. Widmalm, L. Hecht, L. D. Barron* **5349–5351**

Glycan Structure of a High-Mannose Glycoprotein from Raman Optical Activity



A revealing signature: The glycan structure of intact yeast external invertase, a high-mannose glycoprotein used as biocatalyst, was investigated by using Raman optical activity (ROA) spectroscopy. The

conformational preferences present in mannose-containing di- and trisaccharides were found to be preserved in the glycan chains, with secondary polypeptide backbone structure suppressed.



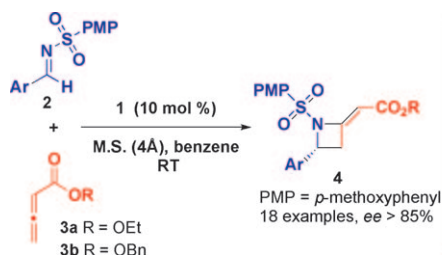
A selective route: Hypermetallyl germanium(II) and tin(II) compounds (see scheme) were prepared using dimethylallyl magnesium reagents and were fully char-

acterized. These derivatives, which contain good leaving substituents, might be suitable candidates for the preparation of nanomaterial alloys.

Group 14 Compounds

N. Katir, D. Matioszek, S. Ladeira, J. Escudié,* A. Castel* — 5352–5355

Stable N-Heterocyclic Carbene Complexes of Hypermetallyl Germanium(II) and Tin(II) Compounds



Mix and go: The quinidine amide **1** catalyzed [2+2] cycloaddition between *N*-sulfonylimines **2** and alkyl 2,3-butadienoates **3** afforded the *R*-configured azetidines **4** in excellent yields and enan-

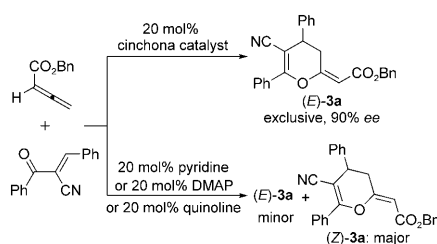
tioselectivities (M.S. = molecular sieve). The *S* enantiomer was obtained when a quinine amide catalyst, the pseudoenantiomer of **1**, was used.

Organocatalysis

J.-B. Denis, G. Masson,* P. Retailleau, J. Zhu* — 5356–5360

Cinchona Alkaloid Amide Catalyzed Enantioselective Formal [2+2] Cycloadditions of Allenates and Imines: Synthesis of 2,4-Disubstituted Azetidines

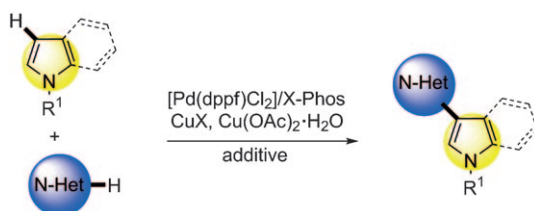
Biologically significant polysubstituted dihydropyrans have been prepared in high to excellent yields and enantioselectivities (see scheme). The interaction between functional groups in the zwitterionic intermediate, which is generated by addition of the amine catalyst to the allenate substrate, is thought to play a crucial role in the stereochemical outcome. Bn = benzyl, DMAP = 4-dimethylamino-pyridine.



Organocatalysis

X. Wang, T. Fang, X. Tong* — 5361–5364

Enantioselective Amine-Catalyzed [4+2] Annulations of Allenates and Oxodienes: An Asymmetric Synthesis of Dihydropyrans



Doubling up: The highly regioselective C3 heteroarylation of either an indole or a pyrrole with an array of electron-rich and electron-poor *N*-heteroarenes has been carried out using a palladium/copper co-

catalytic system. The double C–H activation selectively delivers the unsymmetrical bi-heteroaryl product instead of the homocoupled products.

Cross-Coupling

Z. Wang, K. Li, D. Zhao, J. Lan, J. You* — 5365–5369

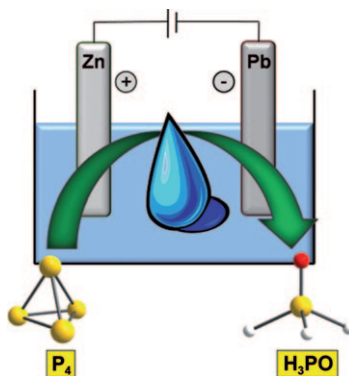
Palladium-Catalyzed Oxidative C–H/C–H Cross-Coupling of Indoles and Pyrroles with Heteroarenes

Phosphorus Chemistry

D. Yakhvarov,* M. Caporali, L. Gonsalvi,
S. Latypov, V. Mirabello, I. Rizvanov,
O. Sinyashin, P. Stoppioni,
M. Peruzzini* _____ 5370–5373



Experimental Evidence of Phosphine Oxide Generation in Solution and Trapping by Ruthenium Complexes



Phosphine oxide (H_3PO), the first defined compound of phosphorus in the oxidation state -1 , was obtained in solution by electrochemical methods starting from white phosphorus (see picture). H_3PO was characterized by NMR solution spectroscopy as a free molecule and isolated as a ligand in ruthenium(II) complexes following tautomerization to phosphinous acid, $\text{H}_2\text{P}(\text{OH})$.

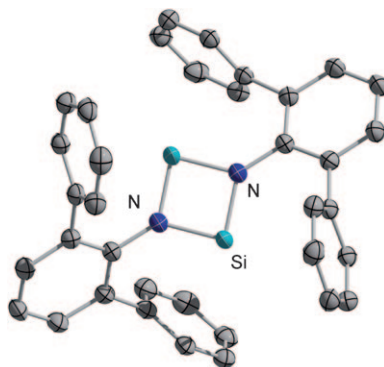


Silicon Chemistry

R. S. Ghadwal, H. W. Roesky,* K. Pröpper,
B. Dittrich, S. Klein,
G. Frenking* _____ 5374–5378



A Dimer of Silaisonitrile with Two-Coordinate Silicon Atoms



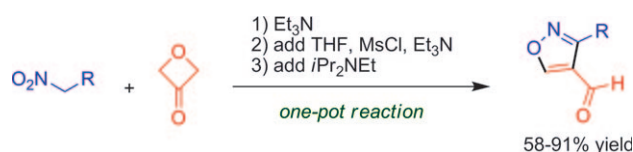
A specialty of silicon: A stable dimeric silaisonitrile (ArNSi)₂ (see picture; Ar = 2,6-bis(2,4,6-triisopropylphenyl)phenyl) was prepared by the reduction of dichlorosilaimine $\text{IPr}\cdot\text{Cl}_2\text{Si}=\text{NAr}$ with KC_8 . The dimer is the first base-free disilylene with two-coordinate silicon atoms; reaction with trimethylsilyl azide affords the first bis(silaimine) ($\text{ArNSi}=\text{NSiMe}_3$)₂ with three-coordinate silicon atoms.

Synthetic Methods

J. A. Burkhard, B. H. Tchitchanov,
E. M. Carreira* _____ 5379–5382



Cascade Formation of Isoxazoles: Facile Base-Mediated Rearrangement of Substituted Oxetanes



Give me five! Nitro compounds and oxetan-3-one react through an intriguing cascade sequence to give isoxazole-4-carbaldehydes using inexpensive reagents

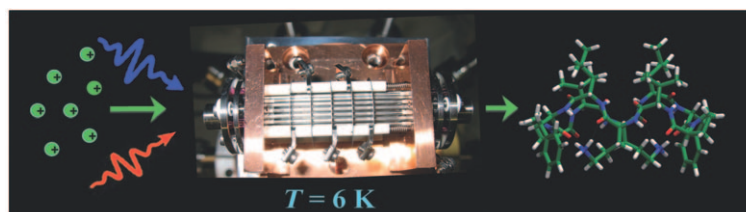
in a one-pot procedure (see scheme; Ms = methanesulfonyl). A variety of 3-substituted isoxazole-4-carbaldehydes were obtained in high overall yields.

Polypeptide Structures

N. S. Nagornova, M. Guglielmi,
M. Doemer, I. Tavernelli, U. Rothlisberger,
T. R. Rizzo, O. V. Boyarkin* - 5383–5386

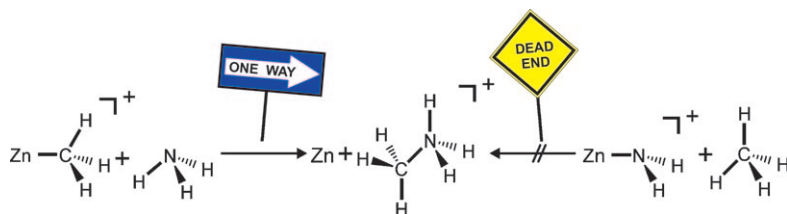


Cold-Ion Spectroscopy Reveals the Intrinsic Structure of a Decapeptide



Trapped, cooled, solved: Cold-ion spectroscopy was used to solve the three-dimensional gas-phase structure of the natural decapeptide gramicidin S. Experiments provide a detailed set of spectroscopic and structural constraints that

unambiguously identify the most stable calculated structure of the isolated peptide. These results provide new information for modeling the biological activity of this antibiotic.



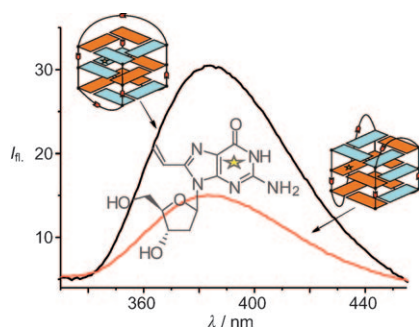
Rally from C to N: The goal of the race concerns connecting carbon and nitrogen. While the $\text{S}_{\text{N}}2$ -type mechanism constitutes a one-way road to produce CH_3NH_3^+

from $\text{Zn}(\text{CH}_3)^+$ and NH_3 , activation of the $\text{C}-\text{H}$ bond of methane in the $\text{Zn}(\text{NH}_2)^+/\text{CH}_4$ system is a blind alley (see scheme).

Gas-Phase Chemistry

R. Kretschmer, M. Schlangen,
 H. Schwarz* _____ 5387–5391

Efficient and Selective Gas-Phase Monomethylation versus N–H Bond Activation of Ammonia by “Bare” $\text{Zn}(\text{CH}_3)^+$: Atomic Zinc as a Leaving Group in an $\text{S}_{\text{N}}2$ Reaction

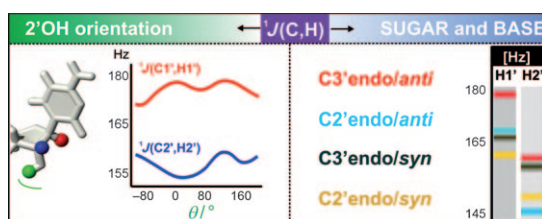


A one light strand: 2'-Deoxyguanosine was made fluorescent by attaching a vinyl group at the C8 position (see structure). The resulting fluorophore is highly sensitive towards DNA double-strand formation and alterations in the secondary structure of its parent oligonucleotide, such as formation of different quadruplex structures. These differences can be readily detected in the emission spectrum (see picture).

Fluorescent Guanine

A. Nadler, J. Strohmeier,
 U. Diederichsen* _____ 5392–5396

8-Vinyl-2'-deoxyguanosine as a Fluorescent 2'-Deoxyguanosine Mimic for Investigating DNA Hybridization and Topology



Pucker up! The 2'OH group in RNA is responsible for the change in the predominant sugar conformation, which is key to the catalytic activity and involved in critical H-bonding interactions. In a combined NMR spectroscopic and quantum chemical investigation, the conforma-

tional dependence of $^1J(\text{C}1',\text{H}1')$ and $^1J(\text{C}2',\text{H}2')$ coupling constants is derived. The precise conformation of the sugar, nucleobase, and the 2'OH group can be determined based on these coupling constants.

RNA Conformations

S. Nozinovic, P. Gupta, B. Fürtig,
 C. Richter, S. Tüllmann,
 E. Duchardt-Ferner, M. C. Holthausen,*
 H. Schwalbe* _____ 5397–5400

Determination of the Conformation of the 2'OH Group in RNA by NMR Spectroscopy and DFT Calculations



Supporting information is available on www.angewandte.org (see article for access details).



A video clip is available as Supporting Information on www.angewandte.org (see article for access details).



This article is available online free of charge (Open Access)

Looking for outstanding employees?

Do you need another expert for your excellent team?
... Chemists, PhD Students, Managers, Professors, Sales Representatives...

Place an advert in the printed version and have it made available online for
1 month, free of charge!

Angewandte Chemie International Edition

Advertising Sales Department: Marion Schulz

Phone: 0 62 01 - 60 65 65

Fax: 0 62 01 - 60 65 50

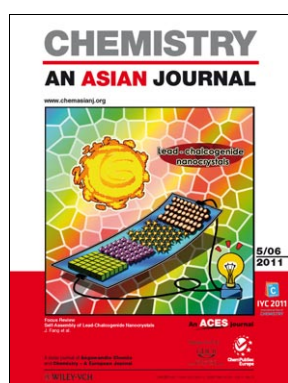
E-Mail: MSchulz@wiley-vch.de

Service

Spotlight on Angewandte's
Sister Journals _____ 5244–5246

Preview _____ 5401

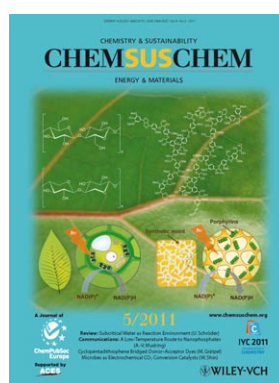
Check out these journals:



www.chemasianj.org



www.chemmedchem.org



www.chemsuschem.org



www.chemcatchem.org

High-Temperature Wetting Transition on Micro- and Nanostructured Surfaces**

Tong Zhang, Jingming Wang,* Li Chen, Jin Zhai, Yanlin Song, and Lei Jiang*

With the discovery of novel wetting phenomena in nature, such as the self-cleaning effect of lotus leaves and the effortless stand and quick waterborne movement of water striders' legs, surfaces with special wettability have recently attracted significant attention and have become increasingly important in our daily lives.^[1] Moreover, surface wettability at non-ambient temperature, especially at high temperature (above 100 °C), is of great importance in many industrial processes, including water transportation and metal processing, among others.^[2] Recently, several advances have been made, such as the fabrication of thermally responsive materials with controllable wettability,^[3] the repellent characteristics of different superhydrophobic surfaces to hot water,^[4] application of hydrophobic surfaces on heat exchangers at low temperature,^[5] evaporation-triggered wetting transition for water droplets on hydrophobic microstructures,^[6] and enhancement of boiling by nanostructured interfaces.^[7] The theory and applications of a liquid droplet bouncing on a hot surface in a solid–liquid heat transfer system, a very important phenomenon, have also been reported.^[8] However, the effect of chemical composition and surface morphology on the wetting behavior at high temperature (above 100 °C) has not been studied systematically.

Herein, we report the investigation of the wetting behavior of surfaces with different chemical compositions and structures from 20 to 200 °C. Four kinds of micro- and nanostructured surfaces with different wettabilities were

successfully fabricated. The wetting behavior of a water droplet was observed to be different on the surfaces, and the wetting transition (from spreading to bouncing) occurred at a specific temperature (i.e., the bouncing temperature, T_b) on hydrophilic, hydrophobic, and superhydrophilic surfaces. Surface wettability was crucial to the wetting-transition behavior, and surface roughness also affected the bouncing temperature of a surface (T_b). When surfaces with the same chemical composition got flatter, T_b decreased at the superhydrophilic surfaces and hydrophobic surfaces, while it increased at the hydrophilic surfaces. However, the spreading–bouncing transition did not take place on superhydrophobic surfaces.

Silicon wafers with various structures were fabricated to investigate wettability at different temperatures. Wafers with micropillars and nanowire arrays (SiNWA) were obtained by lithography etching and chemical etching, respectively.^[9] The samples were coated with fluoroalkylsilane (FAS) to obtain hydrophobic substrates.^[10] Figure 1 shows the top-view scanning electron microscope (SEM) images and the static contact angle (CA) images of a water droplet before and after chemical modification with FAS at 25 °C. As shown in Figure 1 a, b, the unmodified flat silicon and microstructured silicon surfaces (MSis) exhibited hydrophilic characteristics, and the FAS-modified MSis (FAS-MSis) were hydrophobic. Correspondingly, in Figure 1 c, d, the unmodified nanostruc-

[*] Dr. T. Zhang, Dr. L. Chen, Prof. Y. Song, Prof. L. Jiang
 Beijing National Laboratory for Molecular Sciences (BNLMS)
 Key Laboratory of Organic Solids
 Institute of Chemistry, Chinese Academy of Sciences
 Beijing 100190 (P. R. China)
 Fax: (+86) 10-8262-7566
 E-mail: jianglei@iccas.ac.cn

Dr. J. Wang, Prof. J. Zhai
 School of Chemistry and Environment, Beihang University
 Beijing 100191 (P. R. China)
 E-mail: wangjm@buaa.edu.cn

Dr. T. Zhang, Dr. L. Chen
 Graduate School of the Chinese Academy of Sciences
 Beijing 100049 (P. R. China)

[**] We are grateful for financial support by the National Research Fund for Fundamental Key Projects (2010CB934700, 2009CB930404, 2007CB936403, 2009AA03Z339) and the National Natural Science Foundation (20920102036, 20974113). The Chinese Academy of Sciences is gratefully acknowledged. We also thank Zhongwei Sun, Mingjie Liu, and Hao Bai for technical support and helpful discussions.

Supporting information for this article is available on the WWW under <http://dx.doi.org/10.1002/anie.201007262>.

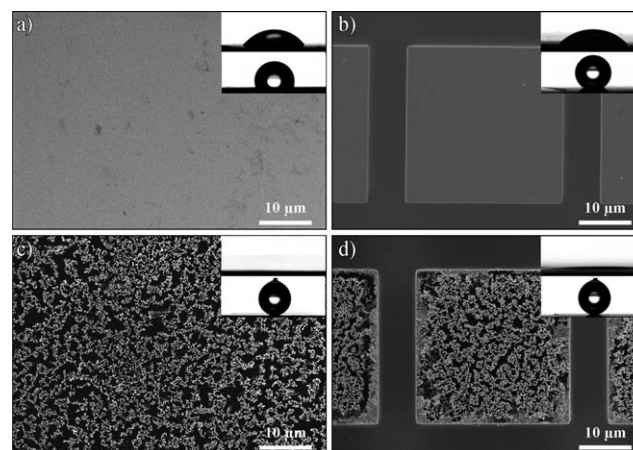


Figure 1. SEM images (top view) of silicon surfaces with hierarchical structure. The insets show the shape of water droplets on these surfaces before (top) and after FAS modification (bottom) at 25 °C. a) Flat silicon wafer. CA (54.2 ± 2.1)°/(106.4 ± 0.5)° (before/after modification) b) Silicon wafer with micropillars. The side length D of the micropillar is 30 μm, CA (41.1 ± 2.5)°/(144.8 ± 0.4)°. c) Silicon wafer with nanowire arrays (SiNWA). CA 0°/(162.2 ± 0.8)°. d) Silicon wafer with the composition of nanowire micropillars. $D = 30$ μm, CA 0°/(166.5 ± 0.7)°.

tured silicon and micro- and nanostructured silicon surfaces (MNSis) were superhydrophilic, with contact angles near 0° , while the FAS-modified MNSis (FAS-MNSis) were superhydrophobic ($CA > 160^\circ$), such that the $2 \mu\text{L}$ water droplet could not descend but was stuck to the pinhead instead. The effect of the micropillar side length D ($D = \infty$ represents surfaces without any microstructure) of the four different substrates on the water contact angle at 25°C are shown in Figure S1 in the Supporting Information.

Subsequently, the wetting behavior of the four groups of surfaces (MSis, FAS-MSis, MNSis, and FAS-MNSis) at various temperatures was investigated. The schematic diagram of the experimental device is shown in Figure S5 in the Supporting Information. A heating stage with controllable temperature was used. The surface temperature and the water spreading or bouncing were recorded with a precise thermocouple and a CCD, respectively. The injector was kept 200 mm higher than the heating stage to preserve the drop from heat. Only when the stage temperature reached the test temperature was the injector rotated down, and a $3.5 \mu\text{L}$ water droplet was pushed out. After the water droplet left the needle of the injector, it was rotated again to the high position. The water droplet was well preserved before coming into contact with the high-temperature surfaces (see the Supporting Information for details).

Figure 2 shows the typical spreading and bouncing behavior of water droplets on surfaces with different wettabilities at temperatures above 100°C . The droplet did not wet the surface but instead bounced on the surface at a certain temperature, which was called the bouncing temperature (T_b). For the hydrophilic smooth silicon surface (Figure 2a), the water droplet stood on the surface with a contact angle smaller than 60° before the surface temperature reached its T_b

at 183°C and then evaporated quickly. When the surface was heated to 183°C or above, the water droplet wetted the surface and then bounced up with a contact time of about 0.16 s. Similarly, T_b of the hydrophobic surface was 164°C . The droplet stood on the hydrophobic smooth silicon surface modified with FAS with a contact angle larger than 100° and evaporated slowly when the surface temperature was lower than its T_b at 164°C (Figure 2b), but bounced up slightly with a longer contact time of about 0.4 s when the temperature reached or exceeded 164°C . In comparison, the droplet evaporated and disappeared immediately when the temperature of the superhydrophilic surface was lower than its T_b at 152°C (Figure 2c). In cases when the surface temperature was higher than 152°C , the droplet on the superhydrophilic surface bounced so strongly and quickly that the contact time between the droplet and the surface was less than 0.04 s. No bouncing occurred on the FAS-modified superhydrophobic surface with SiNWA (Figure 2d). At lower temperatures (e.g., 60°C), the droplet pinned on the surface and evaporated very slowly, but at higher temperature (80°C), below the boiling point of water, the droplet rolled away after being dropped on the surface.

At a given temperature, the vaporizing velocity of a droplet clearly depends on the heat-transfer ability of the surface. The more heat is transferred through the solid-liquid interface, the faster the droplet vaporizes. Hence, the wetting and bouncing processes both indicated that the superhydrophilic surface had excellent heat-transfer ability. The drop evaporated very fast below T_b , and above T_b , the bottom part of the droplet evaporated faster and formed a vapor film to bounce the droplet up in less than 0.04 s, which was much faster than on the hydrophilic and hydrophobic surfaces. In comparison, the droplet stood on the superhydrophobic

surface with a contact angle larger than 150° and evaporated very slowly at lower temperature and did not wet but rolled away at 80°C . The small velocity of vaporization demonstrated the poor heat-transfer ability of the superhydrophobic surface.

Although substrates with similar structures, such as the MSis, exhibited similar high-temperature spreading and bouncing and had similar contact times in the bouncing process, T_b of surfaces with similar contact angles varied with the change of surface roughness. Figure 3 shows the relationship between surface roughness and T_b for MSis, MNSis, and FAS-MSis. With an increase in D (from $10 \mu\text{m}$ to infinity), T_b increased for the hydrophilic MSis (from 157 to 183°C) while it decreased for the hydrophobic FAS-MSis (from 186 to 164°C)

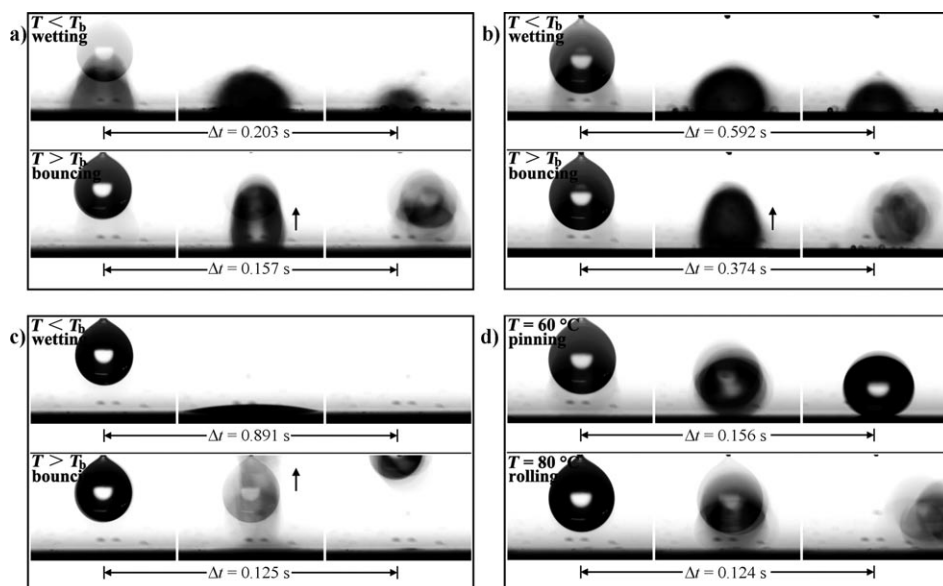


Figure 2. Video snapshots of typical wetting and bouncing behavior of water droplets on high-temperature surfaces. a) Unmodified flat hydrophilic silicon surface, $T_b = 183^\circ\text{C}$. b) FAS-modified flat hydrophobic silicon surface, $T_b = 164^\circ\text{C}$. c) Unmodified superhydrophilic SiNWA, $T_b = 152^\circ\text{C}$. d) FAS-modified superhydrophobic SiNWA surface. No bouncing occurred on this surface.

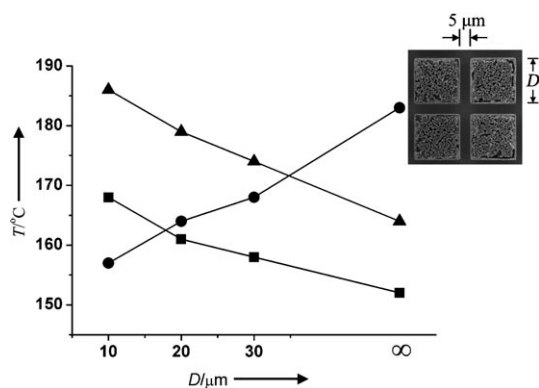


Figure 3. The bouncing temperature (T_b) with different micropillar side lengths D . $D = \infty$ represents the surfaces without any microstructure. ●: Microstructured hydrophilic surfaces (MSis). ▲: Microstructured hydrophobic surfaces (FAS-MSis). ■: Micro- and nanostructured superhydrophilic surfaces (MNSis).

and superhydrophilic MNSis (from 168 to 152 °C). T_b of the hydrophilic MSis was higher than the superhydrophilic MNSis for $D \geq 20 \mu\text{m}$.

The comparisons between the T_b of different surfaces remind us that, although the superhydrophilic MNSis could enhance heat transfer between solid and water, the droplet would bounce on them at a lower temperature compared with the hydrophilic MSis. Furthermore, if the surface temperature is above T_b , a vapor film would be generated. Therefore, for equipment with strict and high working temperature, the surface with a higher T_b should be chosen.

Two theoretical models of the wetting state at high temperature have been proposed to explain the change in T_b (Figure 4). It is understood that a set volume of vapor film has to be produced by phase transition to bounce a given droplet. Throughout the bouncing process, the internal temperature of the water droplets changed little. Therefore, the vaporization velocity and the vapor film formation could only be influenced by the change of surface conditions (Supporting Information S6).^[11] As shown in Figure 4, the volume of vapor film can be expressed as in Equation (1):

$$V = A(v_v - v_w)t \quad (1)$$

where V is the volume of vapor film, A is the wetting area between solid and liquid, v_v is the vaporizing velocity that changes with surface temperature, v_w is the rewetting velocity controlled by the contacting solid and liquid, and t is the time of wetting before bouncing. When the droplet made contact with the unmodified MSis and the MNSis with high surface energy, it was in a Wenzel state, in which the liquid completely fills the grooves of the rough surface.^[12] According to Figure 4a and Equation (1), if V and v_w are invariable and t changes little on similar surfaces, then v_v must decrease with the increase in A , and T_b would decrease as well. For the hydrophilic MSis, the wetting area between silicon and water decreases when D increases (see the Supporting Information). Hence, T_b exhibits the same change as D . For the MNSis, A decreases with a decrease in D , so T_b decreased

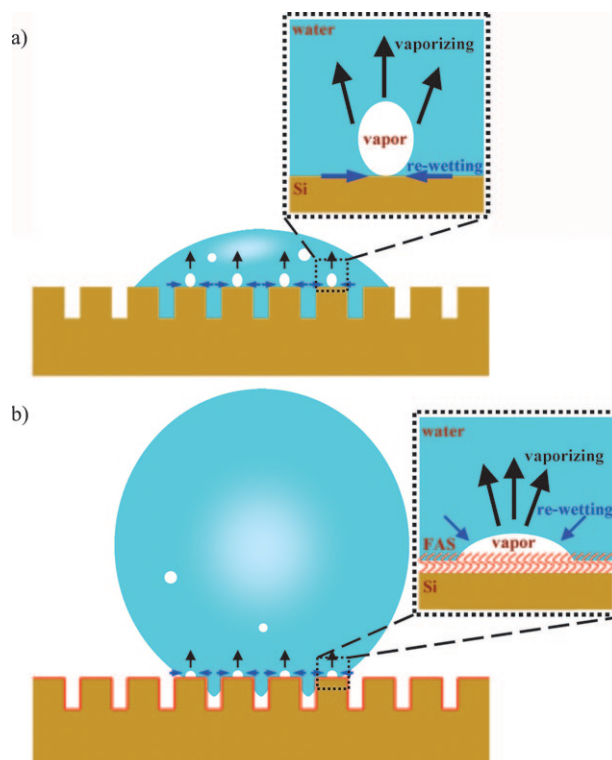


Figure 4. Two proposed mechanisms of the wetting state at high temperature. a) Wetting details of the Wenzel state at high temperature. Air bubbles are generated quickly and escape from the hydrophilic surface easily. b) Wetting details of the Cassie state at high temperature. Air bubbles are generated slowly and prefer to stick on the hydrophobic surface for a longer time.

when D increased. Furthermore, nanostructured surfaces have far larger specific surface areas than microstructured surfaces, so the value of A for MNSis is much larger than that of MSis, which makes t for MNSis much shorter than the other bounced series of surfaces. In contrast, FAS-MSis and FAS-MNSis exhibited the Cassie state when drops made contact with them. In the Cassie state, A becomes larger as the surface gets flatter, because air remains in the micro- and nano-grooves. For FAS-MSis, the longer D is, the larger A becomes, and T_b decreases accordingly. However, according to the Cassie equation, if a surface exhibits excellent superhydrophobic characteristics with a contact angle near 180°, the droplet cannot wet the surface but would be separated from the solid by an almost continuous air film. The Cassie equation is defined as in Equation (2):

$$\cos \theta_c = f_s(\cos \theta + 1) - 1 \quad (2)$$

where f_s is the area fraction of the solid.^[13] If θ_c is close to 180°, then f_s would be quite tiny as it approaches 0. As a result, v_v would be near 0, too. Thus, the droplet could not bounce on the superhydrophobic FAS-MNSis but rolled away with a slight imbalance. More evidence can be seen in Supporting Information.

In summary, the typical wetting transition on micro- and nanostructured surfaces with different wettabilities at high

temperature has been investigated. Experimental results indicate that both surface wettability and surface roughness are crucial to the wetting transition behavior. The spreading–bouncing transition occurred on hydrophilic, hydrophobic, and superhydrophilic surfaces above 100 °C. When the side length of micropillars on substrates increased from 10 μm to infinity (i.e., no micropillars), T_b decreased for the superhydrophilic MNSis and hydrophobic FAS-MSis, while it increased for the hydrophilic MSis. However, the spreading–bouncing transition could not take place on superhydrophobic FAS-MNSis. The two proposed mechanisms of wetting at high temperature explained the transition phenomena well. Moreover, the high-temperature wetting transition could be potentially valuable in water transportation and other industrial applications, such as material choice in liquid–solid systems working at non-ambient temperature.

Experimental Section

Instruments and characterization: SEM images of the samples were obtained using a field-emission scanning electron microscope (JSM-6700F, Japan). Contact angles were measured on an OCA20 instrument (DataPhysics, Germany) at 25 °C. Deionized water droplets (about 2 μL) were dropped carefully onto the surface. The average contact angle value was obtained by measuring at five different positions of the same sample.

Fabrication of SiNWA: Cut silicon wafers were soaked in H₂SO₄/H₂O₂ (H₂SO₄ (97 %)/H₂O₂ (30 %) = 3:1) for 30 min at 80 °C, then rinsed with deionized water four or five times. Cleaned silicon strips were put into the etching solution (HF 5.0 mol L⁻¹ and AgNO₃ 0.015 mol L⁻¹), sealed at 50 °C for 25 min, then immersed in 20 % nitric acid for 30 s and finally rinsed with deionized water four or five times.

Modification with FAS: Cleaned silicon strips with microstructures were put into a sealed container together with a piece of glass coated with about 0.5 mL FAS. Then the container was then evacuated with a vacuum pump, and the vacuum was maintained for 12 h.

Received: November 18, 2010

Revised: February 21, 2011

Keywords: high-temperature chemistry · hydrophobic effect · microstructure · surface chemistry · wettability

- [1] a) M. J. Liu, Y. M. Zheng, J. Zhai, L. Jiang, *Acc. Chem. Res.* **2010**, *43*, 368–377; b) T. L. Sun, L. Feng, X. F. Gao, L. Jiang, *Acc. Chem. Res.* **2005**, *38*, 644–652; c) L. Feng, S. H. Li, Y. S. Li, H. J. Li, L. J. Zhang, J. Zhai, Y. L. Song, B. Q. Liu, L. Jiang, D. B. Zhu, *Adv. Mater.* **2002**, *14*, 1857–1860; d) X. J. Feng, L. Jiang, *Adv. Mater.* **2006**, *18*, 3063–3078; e) F. Xia, L. Jiang, *Adv. Mater.* **2008**, *20*, 2842–2858; f) J. K. Yuan, X. G. Liu, O. Akbulut, J. Q. Hu, S. L. Suib, J. Kong, F. Stellacci, *Nat. Nanotechnol.* **2008**, *3*, 332–336; g) D. Quere, M. Reyssat, *Philos. Trans. R. Soc. London Ser. A* **2008**, *366*, 1539–1556; h) J. B. Boreyko, C. H. Chen, *Phys. Rev. Lett.* **2009**, *103*, 184051.
- [2] a) J. Hashmi, L. Looney, M. S. J. Hashmi, *J. Mater. Process. Technol.* **2001**, *119*, 324–328; b) J. Hashmi, L. Looney, M. S. J. Hashmi, *J. Mater. Process. Technol.* **2001**, *119*, 329–335.
- [3] a) T. L. Sun, G. J. Wang, L. Feng, B. Q. Liu, Y. M. Ma, L. Jiang, D. B. Zhu, *Angew. Chem.* **2004**, *116*, 361–364; *Angew. Chem. Int. Ed.* **2004**, *43*, 357–360; b) N. Wang, Y. Zhao, L. Jiang, *Macromol. Rapid Commun.* **2008**, *29*, 485–489.
- [4] Y. Liu, X. Chen, J. Xin, *J. Mater. Chem.* **2009**, *19*, 5602–5611.
- [5] S. Daniel, M. K. Chaudhury, J. C. Chen, *Science* **2001**, *291*, 633–636.
- [6] P. C. Tsai, R. G. H. Lammertink, M. Wessling, D. Lohse, *Phys. Rev. Lett.* **2010**, *104*, 116102.
- [7] a) S. H. Li, R. Furberg, M. S. Toprak, B. Palm, M. Muhammed, *Adv. Funct. Mater.* **2008**, *18*, 2215–2220; b) R. Chen, M. C. Lu, V. Srinivasan, Z. Wang, H. H. Cho, A. Majumdar, *Nano Lett.* **2009**, *9*, 548–553; c) C. Li, Z. Wang, P. I. Wang, Y. Peles, N. Koratkar, G. P. Peterson, *Small* **2008**, *4*, 1084–1088.
- [8] a) M. Elbahri, D. Paretkar, K. Hirmas, S. Jebril, R. Adelung, *Adv. Mater.* **2007**, *19*, 1262–1266; b) C. T. Avedisian, J. Koplik, *Int. J. Heat Mass Transfer* **1987**, *30*, 379–393; c) J. Bernardin, I. Mudawar, *J. Heat Transfer* **1999**, *121*, 894; d) H. Linke, B. J. Aleman, L. D. Melling, M. J. Taormina, M. J. Francis, C. C. Dow-Hygelund, V. Narayanan, R. P. Taylor, A. Stout, *Phys. Rev. Lett.* **2006**, *96*, 154502; e) A. L. Bianco, C. Clanet, D. Quere, *Phys. Fluids* **2003**, *15*, 1632–1637.
- [9] K. Peng, Y. Yan, S. Gao, J. Zhu, *Adv. Funct. Mater.* **2003**, *13*, 127–132.
- [10] A. Nakajima, A. Fujishima, K. Hashimoto, T. Watanabe, *Adv. Mater.* **1999**, *11*, 1365–1368.
- [11] a) T. Kudra, Y. Pan, A. Mujumdar, *Drying Technol.* **1991**, *9*, 693–707; b) Y. Ge, L. S. Fan, *Int. J. Heat Mass Transfer* **2006**, *49*, 4231–4249; c) N. Nikolopoulos, A. Theodorakakos, G. Bergeles, *Int. J. Heat Mass Transfer* **2007**, *50*, 303–319.
- [12] R. Wenzel, *Ind. Eng. Chem.* **1936**, *28*, 988–994.
- [13] A. Cassie, S. Baxter, *Trans. Faraday Soc.* **1944**, *40*, 546–551.